JOURNAL OF AIRCRAFT
Vol. 44, No. 1, January–February 2007

Robust Multivariable Closed-Loop Control of a Turbulent Backward-Facing Step Flow

Lars Henning and Rudibert King*
Berlin University of Technology, 10623 Berlin, Germany

DOI: 10.2514/1.22934

Active control of separated flows has become an attractive approach enabling the designer to meet increased performance demands for various systems. Whereas a significant part of the work published so far in the area of closed-loop flow control is based on simulation studies, this paper presents an example of a successful application of a multivariable controller in wind tunnel experiments. A robust $\mathcal{H}_\infty$ controller is used to control the spanwise variable reattachment length downstream of a benchmark problem, the backward-facing step. To reduce the conservatism of this approach, a nonlinear static precompensation is included, first. The synthesis of the controller is based on a family of identified linear black-box models, which describe the compensated input/output behavior of the plant. Tracking performance and disturbance rejection of the controller are tested in wind tunnel experiments and shown in this paper.

Nomenclature

$\mathbf{a}(t)$	=	actuation vector
$\mathbf{a}_0(t)$	=	normalized actuation amplitude
$\mathbf{C}(s)$	=	MIMO controller
$\mathbf{d}(t)$	=	disturbance vector
f	=	frequency
f_a	=	actuation frequency
f_s	=	sampling frequency
f_{shear}	=	instability frequency of the shear layer
$\mathbf{G}(s)$	=	model of the plant
$\mathbf{G}_N(s)$	=	nominal model
H	=	step height
$\mathbf{I}$	=	unit matrix
i	=	index
j	=	imaginary unit
$\mathbf{K}_S$	=	static gain
$\mathbf{L}(s)$	=	open-loop transfer function
$l_M(\omega)$	=	minimum distance to all identified models
N	=	cost functional
p'_{rms}	=	root-mean-square value of pressure fluctuations
$\mathbf{q}_{\text{act}}(t)$	=	maximum velocity vector at the actuator slot
Re_H	=	Reynolds number based on step height, $Re_H = Hu_\infty/\nu$
Re_{δ_2}	=	Reynolds number based on boundary layer momentum thickness, $Re_{\delta_2} = \delta_2 u_\infty/\nu$
$\mathbf{r}(t)$	=	reference variable vector
$\mathbf{S}(s)$	=	sensitivity transfer function
St_H	=	Strouhal number based on step height, $St_H = Hf_a/u_\infty$
$St_{x_{Rm}}$	=	Strouhal number based on reattachment length, $St_{x_{Rm}} = x_{Rm}f_a/u_\infty$
St_{δ_2}	=	Strouhal number based on boundary layer momentum thickness, $St_{\delta_2} = \delta_2 f_a/u_\infty$
s	=	Laplace variable
$\mathbf{T}(s)$	=	complementary sensitivity transfer function
t	=	time
t_{rms}	=	averaging time of rms values
$\mathbf{t}_0$	=	time delay vector
$\mathbf{u}(t)$	=	manipulated variable or control input
$u(x, y, z, t)$	=	flow velocity in streamwise direction
u_∞	=	freestream velocity
W	=	step width
$\mathbf{W}_{CS}(s)$, $\mathbf{W}_S(s)$, $\mathbf{W}_T(s)$	=	weights for $\mathcal{H}_\infty$ minimization
w_s	=	width of actuator slots
x, y, z	=	streamwise, transverse, and spanwise coordinates, respectively
$\mathbf{x}_R(t)$	=	reattachment length vector using rms method
$\mathbf{x}_{Rm}$	=	time-averaged reattachment length vector
$\mathbf{x}_{Rm_0}$	=	time-averaged reattachment length vector for the unactuated flow
$\mathbf{y}(t)$	=	control variables or output vector
$\mathbf{\Delta}_M(s)$	=	multiplicative uncertainty
δ_2	=	boundary layer momentum thickness
δ_{99}	=	boundary layer thickness
η	=	viscosity
ν	=	kinematic viscosity
$\sigma_{\min}$, $\sigma_{\max}$	=	minimal and maximal singular values
τ_W	=	wall-shear stress
ω_B	=	bandwidth
ω_C	=	crossover frequency

Received 2 February 2006; revision received 27 October 2006; accepted for publication 27 October 2006.

*Measurement and Control Group, Institute of Process and Plant Technology, Hardenbergstraße 36a; rudibert.king@tu-berlin.de (corresponding author).

I. Introduction

FLOW separations from swept wings with variable chord, in turbomachines, or from bluff bodies, such as automobiles, show complex space- and time-dependent behavior. Flow separation leads to degraded performance such as reduced lift and increased drag of an airfoil, noise production, and efficiency loss in turbines, or decreased pressure behind trucks or ships and, hence, increased aerodynamic drag [1,2]. In combustion chambers, however, a recirculation region

as a result of flow separation is desired to keep the fuel mixture in the reaction zone for an efficient combustion [3].

Thus, control of flow separation is one of the main topics in the fluid dynamics community in the last decade. First, only passive means of flow control were considered [4,5]. However, when shaping of the geometry has reached an optimum, or when passive means, such as vortex generators, have positive and negative effects, active devices can further improve the performance by suction and blowing, acoustic actuation, or magnetohydrodynamic forces [6]. Furthermore, by exploiting flow instabilities, active flow control is able to adapt the actuation to a wide range of operating conditions in an optimal sense, that is, with a minimal energy expenditure [7]. The first real active open-loop flow control demonstration for an airplane was done with a XV-15 tilt-rotor aircraft [8].

Many flow control studies have concentrated on benchmark problems to develop and elucidate the basic principles. Examples are the flow around a cylinder or past a backward-facing step. The backward-facing step flow field and the possible actuation mechanisms are comprehensively described in numerical and experimental studies; see, for example, [9–14].

All these investigations, however, are dedicated to open-loop control, as most of the work published so far on active flow control. Literature surveys on open-loop flow control, including actuation mechanisms and sensor applications, are given in [15–19].

As a natural extension, this contribution focuses on the closed-loop control of separated flows by active means to profit from well-known advantages, such as disturbance rejection and set-point tracking. It differs from the majority of the published work in this field with respect to two important features such as the following:

1) The developed closed-loop controller is applied in a real experiment.

2) It is shown that variable, nonconstant reattachment lines can be controlled, as well, to address problems such as separation control over swept wings with variable chord length in the future.

Different approaches to synthesize closed-loop controllers exist. The most physically based approach starts from the solution of the Navier–Stokes equations (NSE). A necessary linearization and the immense computing power needed to solve the controller equations, however, limits the applicability of this synthesis method. Examples are given in [20–22].

A promising approach capable of alleviating the limitations resulting from the infinite dimensional character of the Navier–Stokes equations are low-dimensional models derived with the intention to synthesize nonlinear controllers. These Galerkin and vortex models for separation control are used, for example, in [23–26].

In recent years, a number of experimental investigations of closed-loop flow control emerged. These are based on the above mentioned low-dimensional or on black-box models of the flow. In [27], a simple low-dimensional model is used to control the flow in the wake of a cylinder. In [28], tuning rules are used for the control of a generic model of an airfoil. The first mode of a proper orthogonal decomposition of an airfoil flow is controlled by a proportional controller in [29]. In [30] a synthesis of robust single-input single-output (SISO) controllers based on identified black-box models for the backward-facing step is shown. A comparison of these SISO controllers with a flatness based, that is, nonlinear controller is given in [31]. In [32], robust and adaptive controllers are compared and used to control the spanwise uniform reattachment length downstream of a backward-facing step, the lift of a generic high-lift configuration, and the pressure recovery in a diffusor flow. Moreover first results concerning the control of the spanwise variable reattachment length upstream of the backward-facing step are provided. Black-box approaches are chosen in experimental burner control studies as well. For example, pressure fluctuations in combustion chambers are controlled in [33]. Tollmien–Schlichting waves are rejected using a finite impulse response (FIR)-based controller in [34] for an airfoil flow. A robust controller and an extremum seeking controller in combination with a model-based sensor, namely, the Kalman filter algorithm, is applied in [35] for drag reduction of a bluff body. Noise suppression of the flow over a cavity is controlled, for example, in [36], or [37]. In [38] a simple linear controller is designed based on a black-box model to control a turbulent jet.

Based on the experience concerning black-box control of various flow geometries, this contribution details the spanwise variable control of the backward-facing step flow.

The paper is organized as follows: The flow configuration is described in Sec. II with an emphasis on the physical processes exploited by the control and on the sensor concept used. Section III summarizes the results of the open-loop control, which form the basis for model identification and controller synthesis which is described in Sec. IV. The results of wind tunnel experiments are discussed in Sec. V, followed by a conclusion and an outlook.

A note on notation: As this contribution is set up at the interface between fluid dynamics and control, a conflict occurs in the nomenclature usually adapted by the two disciplines. To facilitate readability, bold variables are used for control related variables, that is, $\mathbf{u}$ is the control input, whereas u is the streamwise velocity. Likewise, $\mathbf{y}$ represents the control output and y the transverse coordinate.

II. Flow Configuration

A. General Description

A sketch of the flowfield with spanwise segmented actuation is given in Fig. 1, where the incoming flow with the freestream velocity u_∞ detaches at the edge of the step and reattaches downstream. Four different regimes exist in the wake: a recirculation zone, also called separation bubble, the shear layer above the recirculation zone, a reattachment zone, and a newly developing boundary layer downstream of the reattachment zone.

In [11,39,40] the convective instability of the initial shear layer is investigated. Small perturbations are exponentially amplified and convect downstream, so that no self-excitation occurs. This phenomenon was investigated for free shear layers first [41] and is known as Kelvin–Helmholtz instability phenomenon. Amplified perturbations lead to vortex formation and pairing with a natural instability frequency f_{shear}. This instability phenomenon can be found in a range of frequencies. Because of the propagation of the shear layer and the decelerated flow in the downstream direction the natural instability frequency is a function of the position in the x direction; see [11] or [42]. The shear layer rolls up into two-dimensional coherent vortical structures. These vortical structures convect downstream with approximately half of the freestream velocity. Further down, a pairing process can be observed before the coherent structures disaggregate due to the interaction with the wall [43].

The recirculation bubble is characterized by pressure driven inflow and outflow caused by shear layer entrainment. Although negative skin friction, that is, reverse flow, occurs in the recirculation zone, the reattachment position is defined by zero wall-shear stress that is given by

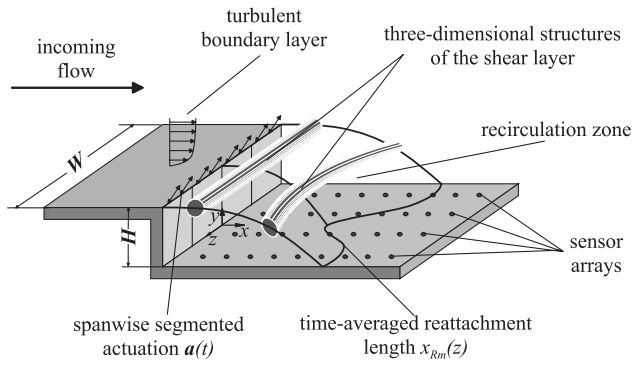

Fig. 1 Configuration of the backward-facing step with four spanwise separated actuators and four sensor arrays for actuation and sensing, respectively.

$$\tau_W = \eta \left(\frac{\partial u}{\partial y} \right) \Big|_{y=0} \quad (1)$$

for isotropic incompressible flows. The velocity in the x direction is given by $u = u(x, y, z, t)$ whereas y is perpendicular to the bottom wall of the step, see Fig. 1. The variable η describes the viscosity of the fluid. Downstream from the reattachment a new boundary layer develops, causing positive skin friction, that is, forward flow.

Periodic blowing and suction at a specific frequency at the backward-facing step edge is an attractive choice for a control input because there is no net mass flow rate provided into the flowfield. Numerous studies have been performed in this direction; see [11,40,44,45], or [15]. In general, it has been found that the growth of roll-up vortices and their interactions, such as pairing, are enhanced at a certain range of actuation frequencies. As a result the reattachment length is reduced. Chun and Sung [12] give a review on the periodic forcing in various backward-facing step configurations.

The vortex generated entrainment mechanism in the shear layer is enhanced by harmonic acoustic actuation of the detaching boundary layer at the edge of the step, as shown in Fig. 1. As the Kelvin–Helmholtz instability is triggered by this chosen input, only a small amount of energy is needed, which leads to an unstable growth of the imposed perturbations. Harmonic actuation is done by periodic sucking and blowing at the edge of the step. The amplitude of the harmonic actuation signal affects the initial size of the growing vortices, the spreading rate of the separated shear layer and, thus, the reattachment length. Hence, the amplitude is chosen as the control input, also called manipulated variable.

Because the reattachment length characterizes the size of the separation bubble, it is taken as the primary variable to be controlled, or the control output. In this benchmark configuration, the goal is to control the reattachment length as a function of the spanwise coordinate z using spanwise segmented actuation. A spanwise variable separation bubble might be of interest for flight control. By implying different spanwise profiles for the lengths of the separated regions above the airfoils on both sides of an airplane, roll moments could be imposed. Because of the very fast dynamics of loudspeakers, or, alternatively, valves or synthetic jets used to modulate a blowing airstream, a much faster response can be obtained compared to rather slow classical mechanical devices, such as control surfaces.

B. Experimental Setup

The experiments are conducted in an "Eiffel"-type wind tunnel. The closed test section is 1600 mm × 88 mm × 400 mm in the streamwise (x), transverse (y), and spanwise (z) directions, respectively. The step is located 27 step heights downstream of the test section inlet, and the step height is $H = 20$ mm. The width of the step equals the entire test section width, that is, $W = 20H$.

All presented experiments are carried out with a step height based Reynolds number $Re_H = Hu_\infty/\nu = 25,000$. The origin of the coordinate system is centered at the lower edge of the step (Fig. 1).

Standard hot-wire measurements are used to measure the incoming boundary layer flow at $x = -0.05H$, using a TSI-IFA 100 constant temperature anemometer. The hot wire is mounted on a one-axis traverse system. The velocities measured with the hot wire are accurate to within 4% and the position of the hot wire is known to within ±0.01 mm. The inlet conditions of the boundary layer and other parameters of the flow configurations are given as follows: Re_H: 25,000; Re_{δ_2}: 1580; δ_{99}/H: 0.68; δ_2/H: 0.06; AR: 20; ER: 1.27; x_{Rm_0}/H: 7.2. Here, the aspect ratio (AR) is defined as the ratio of the step width W to the step height H. The expansion ratio (ER) is given by the ratio of the cross section area downstream to the cross section area upstream of the backward-facing step. The measured time-averaged reattachment length for the unactuated flow is in good agreement with measured values in other investigations (cf. [12] or [6]).

For actuation, slot-hose-loudspeaker systems are used. The actuators are provided with a slot width of $w_s = 0.05H$. The angle of the slot to the streamwise direction is 45 deg, as indicated in Fig. 1. The width of each actuator is $4.5H$. For spanwise segmented actuation, four actuators are positioned in the spanwise direction. Each actuator is connected by hoses to an individually controllable loudspeaker. Here, a harmonic actuation vector, $\mathbf{a}(t) = \mathbf{a}_0(t)\sin(2\pi f_a t)$, with actuation amplitude $\mathbf{a}_0(t)$ and actuation frequency f_a is applied. The vector $\mathbf{a}_0(t)$ is the normalized amplitude vector with $\mathbf{a}_0(t) = [a_{0,1}, a_{0,2}, a_{0,3}, a_{0,4}]^T$. The dimensionless actuation amplitude $\mathbf{a}_0(t)$ is defined as the ratio of the phase and spanwise averaged maximum velocity at each actuator slot $\mathbf{q}_{\text{act}} = [q_{\text{act},1}, q_{\text{act},2}, q_{\text{act},3}, q_{\text{act},4}]^T$ to the freesteam velocity u_∞, that is, $\mathbf{a}_0(t) = \mathbf{q}_{\text{act}}/u_\infty$. To determine $\mathbf{q}_{\text{act}}$, the actuator slot velocities are measured using a standard hot-wire technique. The hot wire is positioned approximately 1 mm inside the slot, while $u_\infty = 0$ ms^{-1}.

The visualization of the time-averaged reattachment length is accomplished by the application of standard oil-film interferometry. The measured time-averaged reattachment lengths are accurate to within ±1 mm.

Data acquisition and implementation of the controller are carried out on rapid prototyping hardware (dSPACE controller board DS1005 PPC) with two A/D boards (dSPACE DS2003, 32 channels, 16 bit resolution) and a D/A board (dSPACE DS2101, five channels, 12 bit resolution). A frequency of $f_s = 5000$ Hz ($f_s H/u_\infty \approx 5.3$) is chosen for data sampling.

C. Sensor Concept

In contrast to many other process control applications, measuring the output signal cannot be done in a straightforward manner in many flow control problems. Although a variety of methods exist in fluid dynamics with which a time-averaged reattachment length can be determined, see for example [46], most of them cannot be used in a closed-loop control setting. Some reasons are insufficient time resolution, missing online capabilities, missing two-dimensional or even one-dimensional information, or simply costs.

As a practical alternative, microphones are used here for surface pressure measurements downstream of the backward-facing step. This method is based on an observation of Mabey [47] that the root-mean-square (rms) value of the pressure fluctuations p'_{rms} downstream of the backward-facing step possess a clear maximum slightly upstream of the mean reattachment location. This characteristic is confirmed in various investigations of separated flows (see [48–51]).

For the experiments considered here, this maximum lies at approximately 86% of the time-averaged reattachment length $\mathbf{x}_{Rm}$, determined by oil-film interferometry, that is, by an averaging technique applying a long averaging time. This is in good agreement with the measurements in [30].

For the measurement of pressure fluctuations, 4 × 15 microphones (Sennheiser, KE 4-211-2) in parallel rows downstream of the step are used. The measured pressure fluctuations are amplified (amplification = 12 dB) and low-pass filtered with a cutoff frequency of 1250 Hz. The microphone rows are located at $z/H = -6.9, -2.3, 2.3$, and 6.9. A distance of $0.625H$ is between the measuring points in the streamwise direction; see Fig. 1. Numerical investigations using large eddy simulations (LES) in comparison with experimental data in [30] have shown that the spatial resolution of the sensor grid is sufficient to resolve the dynamic behavior of the flow. Furthermore, Becker et al. [52] propose a model-based sensor for the tracking of coherent vortical structures based on measured microphone signals.

Figure 2 displays the surface pressure rms values downstream of the step in different spanwise positions for spanwise segmented actuation. The streamwise coordinates are normalized by the time-averaged reattachment length $\mathbf{x}_{Rm} = [x_{Rm,1}, x_{Rm,2}, x_{Rm,3}, x_{Rm,4}]^T$ which is measured at $z/H = -6.9, -2.3, 2.3$, and 6.9, corresponding to the positions of the microphone rows. Although different actuation amplitudes in the spanwise direction are used ($\mathbf{a}_0 = [0.06, 0.02, 0.01, 0.0]^T$), the maxima of p'_{rms} are sufficiently similar with respect to $\mathbf{x}_{Rm}$. From these measurements it can be concluded that by means of an online fit of a fifth-order polynomial to the measured rms values the maxima and thereby the reattachment

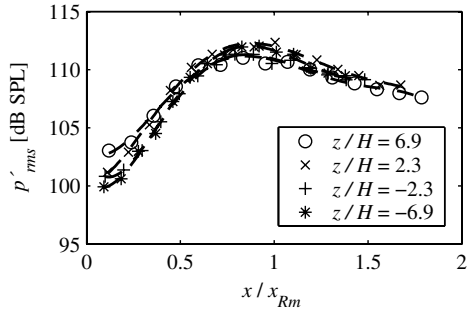

Fig. 2 Relative positions of rms values of the pressure fluctuations using spanwise segmented actuation with $St_H = 0.3$ and $\mathbf{a_0} = [0.06, 0.02, 0.01, 0.0]^T$.

length components in $\mathbf{x}_R(t) = [x_{R,1}, x_{R,2}, x_{R,3}, x_{R,4}]^T$ can be estimated. This method is called the rms method in the following.

It has to be pointed out, however, that the rms method does not resolve all time scales of the dynamic behavior of the reattachment length as it includes a short time averaging in the determination of the rms values. For system identification and controller design, as described below, an averaging time of $t_{\text{rms}} = 1.5$ s ($t_{\text{rms}} u_\infty / H \approx 1400$) is chosen. For a shorter averaging time, a constant relation between the location of the maxima of the p'_{rms} and $\mathbf{x}_{Rm}$ is not observable. This is crucial in as far as the processes which decisively influence the length and the form of the recirculation zone proceed at very high speeds. To obtain finer resolution, other methods, for example, by exploiting model-based measuring techniques [52], or other measurement devices, such as very sensitive pressure taps [35], are needed. In [32] an array of low-pressure sensors is applied in the centerline downstream of the backward-facing step to obtain the reattachment length much faster. However, not enough pressure sensors were available for this investigation to equip four sensor lines.

The rms method, therefore, can only be used to measure rather slow processes, such as those imposed by set-point changes in a closed-loop control setting.

III. Open-Loop Characteristics

The main objective of the open-loop experiments is to explore the effect of the actuation. First, spanwise uniform actuation is used to determine the optimal actuation frequency and to analyze the effect of the actuation amplitude. Afterwards, the effect of spanwise segmented actuation is considered.

For spanwise uniform actuation, the actuation amplitude is given by a scalar a_0, that is, all loudspeakers are driven by the same voltage. The term x_{Rm} represents the spanwise- and time-averaged reattachment length in the open-loop controlled and x_{Rm_0} the spanwise- and time-averaged reattachment length for the unactuated case. Figure 3 shows the normalized time-averaged reattachment length x_{Rm}/x_{Rm_0} as a function of the step height based Strouhal

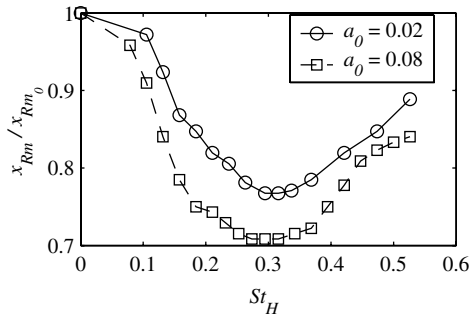

Fig. 3 Normalized time-averaged reattachment length x_{Rm}/x_{Rm_0} as a function of the Strouhal number St_H. Spanwise uniform actuation with $a_0 = 0.02$ and $a_0 = 0.08$.

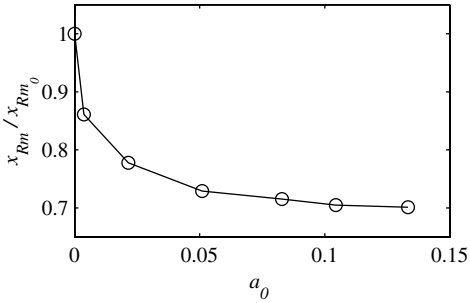

Fig. 4 Normalized time-averaged reattachment length x_{Rm}/x_{Rm_0} as a function of the normalized actuation amplitude a_0. Spanwise uniform actuation with $St_H = 0.3$.

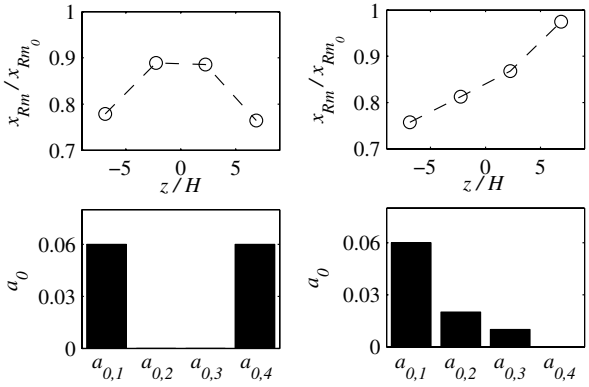

Fig. 5 Normalized time-averaged reattachment length using spanwise segmented actuation with $St_H = 0.3$ for two different cases (top figures). Corresponding actuation amplitudes in $\mathbf{a_0}$ are shown in the bottom figures.

number St_H for two different actuation amplitudes, $a_0 = 0.02$ and $a_0 = 0.08$. A pronounced minimum exists for Strouhal number $St_H = 0.3$, which is independent of the actuation amplitude. This frequency is used as the optimal actuation frequency in the following. It is approximatively in agreement with [12]. Hence, an optimal boundary layer momentum thickness based Strouhal number is given by $St_{\delta_2} = 0.017$. In [6] a reduced frequency based on the time-averaged reattachment length in the form $St_{x_{Rm}} = x_{Rm} f_a / u_\infty$ is proposed. Here, the authors specify an optimal excitation frequency range of $1.5 \leq St_{x_{Rm}} \leq 2.0$ which is in agreement with various separation control experiments. In correspondence to this reference the optimal reduced frequency is given with $St_{x_{Rm}} = 1.6$ in this contribution.

In Fig. 4, the normalized time-averaged reattachment length x_{Rm}/x_{Rm_0} is plotted as a function of the actuation amplitude, where spanwise uniform actuation in which the optimal frequency $St_H = 0.3$ is used. It can be observed that the time-averaged reattachment length is highly sensitive in the amplitude range $0 \leq a_0 \leq 0.05$. For $a_0 > 0.05$, no further effective reduction of the reattachment length can be achieved. The maximum reduction in comparison to the unactuated case is approximately 30%.

For spanwise segmented actuation, different combinations of the vector-valued actuation amplitude $\mathbf{a}_0$ are applied. Figure 5 shows two out of many different experimentally obtained situations for actuation with $\mathbf{a}_0 = [0.06, 0.0, 0.0, 0.06]^T$ on the left, and $\mathbf{a}_0 = [0.06, 0.02, 0.01, 0.0]^T$ on the right. The normalized time-averaged reattachment lengths $\mathbf{x}_{Rm}/\mathbf{x}_{Rm_0}$ as a function of z/H are shown in the upper plots. The actuation amplitudes in $\mathbf{a}_0$ are given by the shaded bars in the lower plots. In the right plot, an inclined profile of the reattachment line is given, whereas in the left plot a symmetric reduction is obtained with a higher reduction on both ends.

Both examples show the possibility to structure the time-averaged reattachment length downstream of the backward-facing step. Furthermore, in the left example coupling effects can be observed.

Although the two inner speakers do not actuate the flow, a reduction of the recirculation length in the inner part behind the step is observed, too. This is an indication of a multiple-input/multiple-output (MIMO) characteristic of the process, which has to be accounted for the controller synthesis, as will be shown in the next section.

IV. Model Identification and Controller Synthesis

Many if not all real systems can only be described in an approximate manner by mathematical models. In this study, the process is described by black-box models, that is, only the input/output behavior is examined. The control input or manipulated variable $\mathbf{u}(t) = [u_1, u_2, u_3, u_4]^T$ corresponds to the actuation amplitude $\mathbf{a}_0(t)$, and the output or control variable $\mathbf{y}(t)$ is described by the reattachment length $\mathbf{x}_R(t)$ obtained by the rms method over the four sensor lines. Thus, a 4×4 MIMO system with four inputs and four outputs is considered. As the normalized actuation amplitude $\mathbf{a}_0$ or the slot velocity $\mathbf{q}_{\text{act}}$ cannot be influenced directly by the controller, the voltage signal driving the loudspeakers is used instead. As a consequence, the models identified in the following comprise both the flow system and the slot-hose-loudspeaker actuators.

To identify linear black-box models, classical step experiments are performed. Thereby each element of the actuation amplitude $\mathbf{a}_0(t)$ is switched successively from zero to different levels or from different levels back to zero to obtain different operating points of the system. A family of 50 linear time-continuous multivariable models of fourth order with a time delay vector $\mathbf{t}_0 = [t_{0,1}, t_{0,2}, t_{0,3}, t_{0,4}]^T$, in the form

$$\begin{aligned} \dot{\mathbf{x}}(t) &= \mathbf{A}\mathbf{x}(t) + \mathbf{B}\begin{pmatrix} u_1(t-t_{0,1}) \\ \vdots \\ u_4(t-t_{0,4}) \end{pmatrix}, \qquad \mathbf{x} \in \Re^4 \\ \mathbf{y}(t) &= \mathbf{C}\mathbf{x}(t) + \mathbf{D}\begin{pmatrix} u_1(t-t_{0,1}) \\ \vdots \\ u_4(t-t_{0,4}) \end{pmatrix} \end{aligned} \tag{2}$$

is fitted to the measured data by the application of subspace methods to determine the entries of the matrices $\mathbf{A}$, $\mathbf{B}$, $\mathbf{C}$, and $\mathbf{D}$; see [53] for details. For the use of frequency-based methods, these models are Laplace transformed, yielding

$$\mathbf{G}_i(s) = \mathbf{C}_i(s\mathbf{I} - \mathbf{A}_i)^{-1}\mathbf{B}_i + \mathbf{D}_i \tag{3}$$

where $\mathbf{A}_i$, $\mathbf{B}_i$, $\mathbf{C}_i$, and $\mathbf{D}_i$ are the matrices identified in a single step experiment. For ease of notation, the influence of the time delay $\mathbf{t}_0$ is not given in Eq. (3). From all identified models $\mathbf{G}_i(s)$, a nominal model $\mathbf{G}_N(s)$ is generated, which shows a minimum distance, here $l_M(\omega)$, to all identified models over a certain frequency range. The plant $\mathbf{G}(s)$, on which the robust controller synthesis is based, is then described by a multiplicative uncertainty $\mathbf{\Delta}_M(j\omega)$ [54]:

$$\mathbf{G}(s) = \mathbf{G}_N(s)[\mathbf{I} + \mathbf{\Delta}_M(s)], \qquad \|\mathbf{\Delta}_M(j\omega)\| \le l_M(\omega) \tag{4}$$

Here, $\mathbf{\Delta}_M(s)$ comprises all models, which, at each frequency ω, are less than or equal to $l_M(\omega)$ in magnitude. The uncertainty is the result of the system described by a simple linear, fourth order models for this nonlinear system.

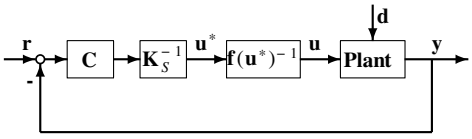

Fig. 7 Control loop with the precompensators $\mathbf{K}_S^{-1}$ for steady-state decoupling and the compensation of the nonlinear static map $\mathbf{f}(\mathbf{u}^*)^{-1}$ (r: reference command; C: controller; u*: manipulated variable; u: compensated manipulated variable; d: disturbances; y: output).

The nonlinearity of the investigated backward-facing step flow causes a widespreading of the model parameters in $\mathbf{G}_i(s)$ and, hence, large values of $l_M(\omega)$. Therefore, a conservative controller design is required for robust closed-loop stability. Analyzing the identified linear model family, a correlation between the amplitudes used for the step experiments and the values of the diagonal elements of the static gain matrix $\mathbf{K}_S = \mathbf{G}_N(0)$ for different actuation amplitudes can be found. This dependency can be approximated by a static map $f_i(u_i) = \mathbf{K}_{S,ii}(u_i)$ for each single input i. Using the inverse functions of these static maps f_i^{-1}, the uncertainty of the models can be partially compensated. The inverse static maps $\mathbf{f}^{-1} = [f_1^{-1}, f_2^{-1}, f_3^{-1}, f_4^{-1}]^T$ are implemented in the control loop as lookup tables with linear interpolation; see Fig. 7. Figure 6 shows a comparison of singular values of all models $\mathbf{G}_i(j\omega)$ computed with compensated and noncompensated models. Maximal and minimal singular values describe the frequency dependent maximal and minimal amplification of a multivariable system, for which the amplification depends on the direction of the vector-valued input signal [54].

The control loop is extended next by a second precompensator for steady-state decoupling, which counteracts the interaction in the plant, yielding four almost independent input–output pairings in the static case; see Fig. 7. This precompensator corresponds to the inverse of the static gain matrix of the nominal model $\mathbf{K}_S^{-1} = \mathbf{G}_N^{-1}(0)$.

For such uncertain systems, many mature controller synthesis methods do exist. Here, a $\mathcal{H}_\infty$-synthesis scheme is chosen. In $\mathcal{H}_\infty$ control, stability and/or performance of the "worst" plant used to describe the process can be guaranteed. To find a tradeoff between the closed-loop sensitivity function $\mathbf{S}(s)$, giving the performance, the restriction of the magnitude of the plant input signals, given by the transfer function $\mathbf{C}(s)\mathbf{S}(s)$, and robustness, given by the complementary sensitivity $\mathbf{T}(s) = \mathbf{I} - \mathbf{S}(s)$, the mixed sensitivity problem is solved. Here, the sensitivity transfer function is given by $\mathbf{S}(s) = \mathbf{I}[\mathbf{I} + \mathbf{L}(s)]^{-1}$, with the open-loop transfer function $\mathbf{L}(s) = \mathbf{C}(s)\mathbf{G}_N(s)$. In doing so, closed-loop transfer functions are weighted with $\mathbf{W}_T(s)$, $\mathbf{W}_{CS}(s)$, and $\mathbf{W}_S(s)$ depending on the frequency, and then combined to a cost functional

$$\min_{\mathbf{C}} \|N(\mathbf{C}(s))\|_\infty, \qquad N = \begin{bmatrix} \mathbf{W}_T(s)\mathbf{T}(s) \\ \mathbf{W}_{CS}(s)\mathbf{C}(s)\mathbf{S}(s) \\ \mathbf{W}_S(s)\mathbf{S}(s) \end{bmatrix} \tag{5}$$

to be minimized, where $\mathbf{C}(s)$ is the optimal controller.

Gains of the identical elements of the weights in diagonal weight matrices are displayed in Fig. 8. For robust stability the weight $\mathbf{W}_T(s)$ is designed, so that $\sigma_{\max}(\mathbf{W}_T(j\omega))$ is an upper bound of $l_M(\omega)$

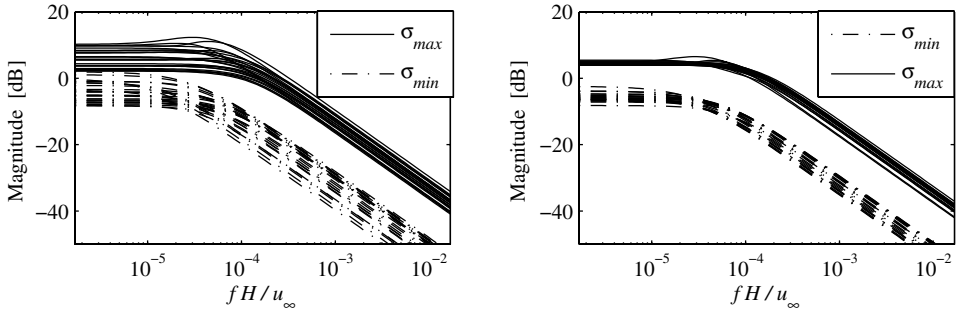

Fig. 6 Singular values of identified models. Noncompensated models (left) in comparison with compensated models (right).

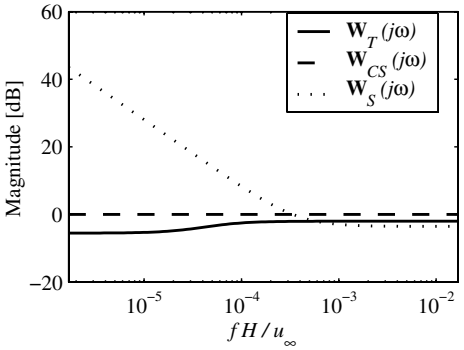

Fig. 8 Examples of gains of single elements of the weights $\mathbf{W}_T(j\omega)$, $\mathbf{W}_{CS}(j\omega)$, and $\mathbf{W}_S(j\omega)$ for the mixed-sensitivity controller synthesis.

for all frequencies, mathematically written as

$$\sigma_{\max}(\mathbf{W}_T(j\omega)) \geq l_M(\omega) \quad \forall\ \omega \tag{6}$$

It is shown that the uncertainty is approximately -6 dB ($\widehat{=}50\%$) in the lower frequency range and increases up to approximately -2 dB ($\widehat{=}80\%$) for $fH/u_\infty \geq 3 \times 10^{-4}$ ($\omega \geq 1.8$ rad/s). Consequently, the uncertainty represented by $\mathbf{W}_T(s)$ is the strongest limitation for the $\mathcal{H}_\infty$-controller approach and a sufficient closed-loop performance only can be achieved for $fH/u_\infty \leq 3 \times 10^{-4}$. To restrict the magnitude of the plant input signal and to consider an actuator limitation the unit matrix $\mathbf{I}$ is selected for the weight $\mathbf{W}_{CS}(s)$. The sensitivity transfer function $\mathbf{S}(s)$ is a good indicator for closed-loop performance. Typical requirements are small maximal singular values $\sigma_{\max}(\mathbf{S}(j\omega))$ at lower frequencies for minimal tracking error and a good disturbance rejection. According to this the diagonal elements of the weight $\mathbf{W}_S(s)$ are designed as illustrated in Fig. 8, where $1/|\mathbf{W}_{S,ii}(j\omega)|$ is the upper bound on $|\mathbf{S}_{ii}(j\omega)|$ for $i = 1 \cdots 4$. For more details of the $\mathcal{H}_\infty$-controller design the reader is referred to standard textbooks, for example, [54].

The result of the $\mathcal{H}_\infty$-controller design is plotted in Fig. 9. The frequency response of the synthesized controller shows an integral behavior in the lower frequency range and can be approximated by a simple proportional plus integral (PI) controller. The crossover frequency ω_C of the nominal open loop $\mathbf{L}(s) = \mathbf{C}(s)\mathbf{G}_N(s)$ is defined as where $\sigma_{\max}(\mathbf{L}(j\omega))$ crosses the 0 dB line from above. Here, the crossover frequency is given at $fH/u_\infty \approx 1.3 \times 10^{-4}$ ($\omega_C \approx 0.8$ rad/s). This relative slow performance is the result of both, the plants uncertainty and the use of the rms method with the long averaging time. The closed-loop bandwidth ω_B is defined as where $\sigma_{\max}(\mathbf{T}(j\omega))$ crosses the -3 dB line form above and is given at $fH/u_\infty \approx 1.2 \times 10^{-4}$ ($\omega_B \approx 0.7$ rad/s).

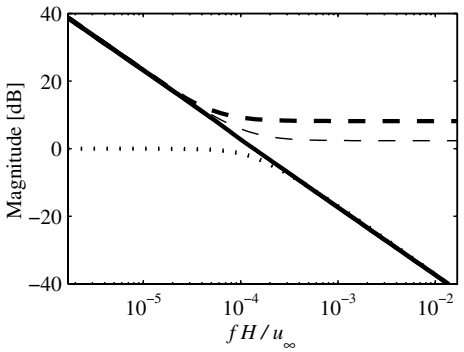

Fig. 9 Singular values of synthesized $\mathcal{H}_\infty$ controller $\mathbf{C}(s)$, open loop $\mathbf{L}(s)$, and complementary sensitivity $\mathbf{T}(s)$; bold dashed line: $\sigma_{\max}(\mathbf{C}(j\omega))$; dashed line: $\sigma_{\min}(\mathbf{C}(j\omega))$; bold solid line: $\sigma_{\max}(\mathbf{L}(j\omega))$; solid line: $\sigma_{\min}(\mathbf{L}(j\omega))$; bold dotted line: $\sigma_{\max}(\mathbf{T}(j\omega))$; dotted line: $\sigma_{\min}(\mathbf{T}(j\omega))$.

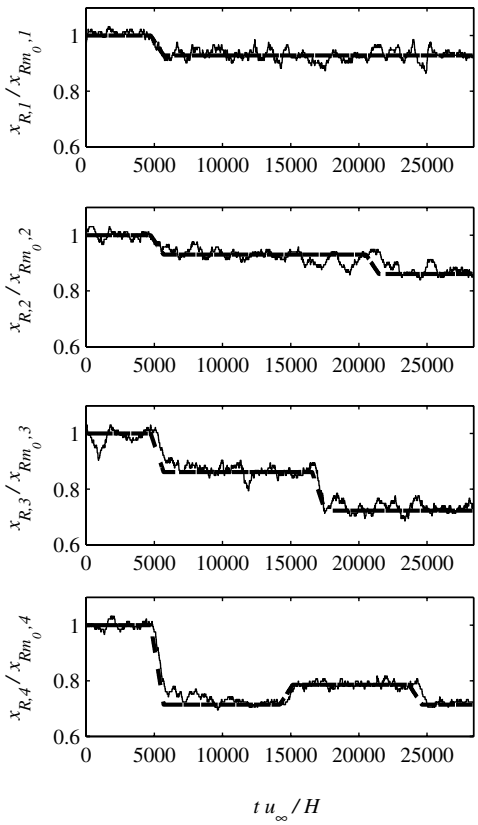

Fig. 10 Tracking response for 4×4 MIMO-control system at $Re_H = 25,000$. Reference command (dashed lines), normalized recirculation length (solid lines).

V. Experimental Results

The behavior of the closed-loop control of the 4×4 MIMO-control system is tested in numerous wind tunnel experiments with respect to tracking response and disturbance rejection.

The plots in Fig. 10 display, for example, the tracking responses of the closed loop applying the synthesized $\mathcal{H}_\infty$ controller at $Re_H = 25,000$. Shown are a time series of the normalized recirculation length $\mathbf{x}_R/\mathbf{x}_{Rm_0}$ (solid lines) above the four sensor arrays and respective independent reference commands (dashed lines). A good tracking performance can be observed. However, the controlled reattachment lengths follow the reference commands with a delay due to the limited temporal resolution of the measurements of $\mathbf{x}_R(t)$. Because of the averaging for the rms calculations, the temporal resolution of the rms method limits the achievable performance. Hence, rampwise changes of the reference command are advised, as with the rms method stepwise changes do not make sense.

A main advantage of closed-loop control in comparison to open-loop control is disturbance rejection. One of several tested possibilities to massively disturb the backward-facing step flow is to reduce the cross-sectional area of the wind tunnel test section at the outflow. The plots of Fig. 11 display the behavior of the normalized reattachment length $\mathbf{x}_R/\mathbf{x}_{Rm_0}$ after placing a cuboid-shaped body ($7.5H \times 5H \times 2.5H$) in the wake of the backward-facing step, at $x/H = 20$. This corresponds to a reduction of the cross-sectional area of approximately 35%. The influence of the disturbance on the flow can be observed in the time series of the Reynolds number, shown in the upper plot. The reference command is set throughout the experiment to be constant, but with spanwise different values, $\mathbf{r} = \mathbf{x}_R/\mathbf{x}_{Rm_0} = [0.93, 0.86, 0.79, 0.71]^T$. In the time interval $0 \leq tu_\infty/H \leq 8000$, the flow is not disturbed, with $Re_H = 25,000$. The manual positioning of the body in the time interval $8000 \leq tu_\infty/H \leq 16,000$ leads to large fluctuations of the Reynolds number. A larger control error can be observed during that period. After the body is in place ($tu_\infty/H \geq 16,000$) the closed-loop control is able to quickly compensate for the effects of this

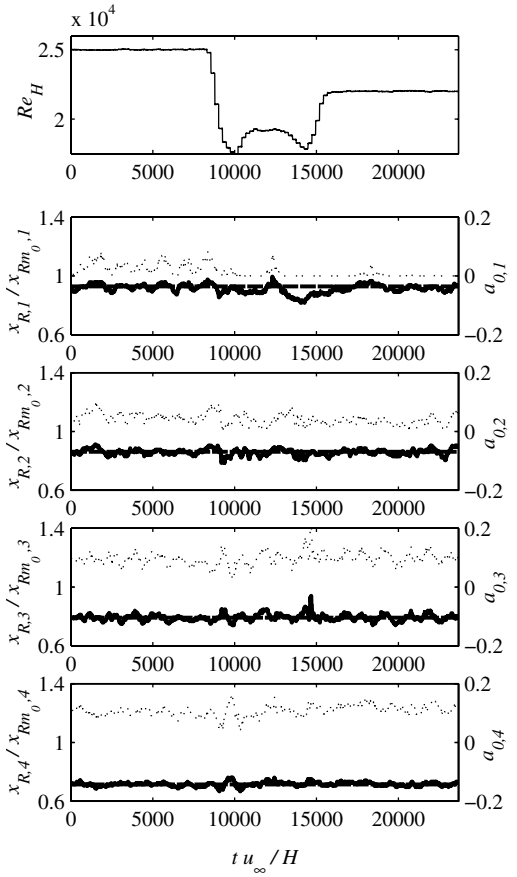

Fig. 11 Disturbance rejection with a massive disturbance by an approximately 35% reduction of the cross-sectional area of the wind tunnel test section. Reference command (dashed lines), normalized recirculation length and Reynolds number (solid lines), normalized actuation amplitude (dotted lines).

disturbance. This experiment shows the superiority of closed-loop control in contrast to open-loop control. When the well-defined conditions of a wind tunnel are replaced by an application in a natural environment, all flow control problems will have to tackle situations in which disturbances act on the system. Hence, only by applying closed-loop control concepts can the benefits of active flow control be fully exploited.

VI. Conclusion and Outlook

The examples presented in this paper show that robust controller synthesis methods can be used to construct and experimentally validate flow controllers. The proposed methodology uses simple black-box models with static precompensation of the nonlinear gain. The synthesized robust controller works for the control of the spanwise variable and time-averaged reattachment length, as demonstrated experimentally.

The dynamic behavior of the closed-loop control is affected by the used rms method for identifying the reattachment location. A faster behavior can be expected by the application of sensor concepts with higher temporal and spatial resolution, such as micro-electro-mechanical systems (MEMS), miniature amplified low-pressure sensors [32], or model-based estimation schemes [52].

In future investigations, the applied methods will be extended to more complex, three-dimensional flow configurations, for example, a swept high-lift configuration, or a bluff body, such as the "Ahmed body."

Acknowledgment

This work was funded by the German Science Foundation (DFG) as part of the Collaborative Research Center (Sfb 557) "Control of complex turbulent shear flows."

References

[1] Simpson, R. L., "Aspect of Turbulent Boundary Layer Separation," *Progress in Aerospace Sciences*, Vol. 32, No. 5, 1996, pp. 457–521.

[2] Hucho, W.-D., *Aerodynamic of Road Vehicles*, 5th ed., Vieweg, Wiesbaden, 2005.

[3] Paschereit, C. O., Gutmark, E., and Weisenstein, W., "Excitation of Thermoacoustic Instabilities by the Interaction of Acoustics and Unstable Swirling Flow," *AIAA Journal*, Vol. 38, No. 6, 2000, pp. 1025–1034.

[4] Tanner, M., "A Method of Reducing the Base Drag of Wings with Blunt Trailing Edges," *Aeronautical Quarterly*, Vol. 23, 1972, pp. 15–23.

[5] Tombazis, N., and Bearman, P. W., "A Study of Three-Dimensional Aspects of Vortex Shedding from a Bluff Body with a Mild Geometric Disturbance," *Journal of Fluid Mechanics*, Vol. 330, 1997, pp. 85–112.

[6] Greenblatt, D., and Wygnanski, I., "The Control of Flow Separation by Periodic Excitation," *Progress in Aerospace Sciences*, Vol. 36, No. 7, 2000, pp. 487–545.

[7] Seifert, A., Bachar, T., Wygnanski, I., Kariv, A., Cohen, H., and Yoeli, R., "Application of Active Separation Control to a Small Unmanned Air Vehicle," *Journal of Aircraft*, Vol. 36, 1999, pp. 474–477.

[8] Wygnanski, I., "The Variables Affecting the Control of Separation by Periodic Excitation," AIAA Paper 2004-2505, 2004.

[9] Kim, J., Kline, S. J., and Johnston, J. P., "Investigation of a Reattaching Turbulent Shear Layer: Flow over a Backward-Facing Step," *Journal of Fluids Engineering*, Vol. 102, 1980, pp. 302–308.

[10] Ruderich, R., and Fernholz, H. H., "An Experimental Investigation of a Turbulent Shear Flow with Separation, Reverse Flow and Reattachment," *Journal of Fluid Mechanics*, Vol. 163, 1985, pp. 283–322.

[11] Hasan, M. A. Z., "The Flow over a Backward-Facing Step Under Controlled Perturbation: Laminar Separation," *Journal of Fluid Mechanics*, Vol. 238, 1992, pp. 73–96.

[12] Chun, K. B., and Sung, H. J., "Control of Turbulent Separated Flow over a Backward-Facing Step by Local Forcing," *Experiments in Fluids*, Vol. 21, No. 6, 1996, pp. 417–426.

[13] Wengle, H., Bärwolff, G., Janke, G., and Huppertz, A., "The Manipulated Transitional Backward-Facing Step Flow: An Experimental and Direct Numerical Simulation Investigation," *European Journal of Mechanics. B Fluids*, Vol. 20, No. 1, 2001, pp. 25–46.

[14] Jürgens, W., and Kaltenbach, H.-J., "Eigenmode Decomposition of Turbulent Velocity Fields Behind a Swept, Backward-Facing Step," *Journal of Turbulence*, Vol. 4, No. 018, 2003, pp. 1–21.

[15] Fiedler, H.-E., and Fernholz, H. H., "On Management and Control of Turbulent Shear Flows," *Progress in Aeronautical Sciences*, Vol. 27, No. 44, 1990, pp. 305–387.

[16] Gad-el-Hak, M., and Bushnell, D. M., "Separation Control: Review," *Journal of Fluids Engineering*, Vol. 113, 1991, pp. 5–29.

[17] Wygnanski, I., and Seifert, A., "The Control of Separation by Periodic Oscillations," AIAA Paper 1994-2608, 1994.

[18] Wygnanski, I., "Boundary Layer and Flow Control by Periodic Addition of Momentum," AIAA Paper 1997-2117, 1997.

[19] Gad-el-Hak, M., Pollard, A., and Bonnet, J.-P., *Flow Control—Fundamentals and Practices*, Springer, Berlin, Heidelberg, 1998.

[20] Choi, H., Moin, P., and Kim, J., "Active Turbulence Control for Drag Reduction in Wall-Bounded Flows," *Journal of Fluid Mechanics*, Vol. 262, 1994, pp. 75–110.

[21] Bewley, T. R., and Liu, S., "Optimal and Robust Control and Estimation of Linear Paths to Transition," *Journal of Fluid Mechanics*, Vol. 365, 1998, pp. 305–349.

[22] Kang, S., and Choi, H., "Suboptimal Feedback Control of Turbulent Flow over a Backward-Facing Step," *Journal of Fluid Mechanics*, Vol. 463, 2002, pp. 201–227.

[23] Coller, B. D., Noack, B. R., Narayanan, S., Banaszuk, A., and Khibnik, A. I., "Reduced-Basis Model of Active Separation Control in a Planar Diffusor Flow," AIAA Paper 2000-2562, 2000.

[24] Wee, D., Park, S., Miake-Lye, R., Annaswamy, A. M., and Ghoniem, A. F., "Reduced Order Modeling of Reacting Shear Layers," AIAA Paper 2002-0478, 2002.

[25] Gerhard, J., Pastoor, M., King, R., Noack, B., Dillmann, A., Morzynski, M., and Tadmor, G., "Model-Based Control of Vortex Shedding Using Low-Dimensional Galerkin Models," AIAA Paper 2003-4262, 2003.

[26] Pastoor, M., King, R., Noack, B., Dillmann, A., and Tadmor, G., "Model-Based Coherent-Stucture Control of Turbulent Shear Flows Using Low-Dimensional Vortex Models," AIAA Paper 2003-4261, 2003.

[27] Siegel, S., Cohen, K., and McLaughlin, T., "Experimental Variable Gain Feedback Control of a Cylinder Wake," AIAA Paper 2004-2611, 2004.

[28] Allan, B. G., Juang, J.-N., Raney, D. L., Seifert, A., Pack, L. G., and Brown, D. E., "Closed-Loop Separation Control Using Oscillatory Flow Excitation," ICASE Rept. 2000-32, 2000.
[29] Glauser, M. N., Higuchi, H., Ausseur, J., and Pinier, J., "Feedback Control of Separated Flows," AIAA Paper 2004-2521, 2004.
[30] Becker, R., Garwon, M., Gutknecht, C., Bärwolff, G., and King, R., "Robust Control of Separated Shear Flows in Simulation and Experiment," *Journal of Process Control*, Vol. 15, No. 6, 2005, pp. 691–700.
[31] Becker, R., and King, R., "Comparison of a Robust and a Flatness Based Control for a Separated Shear Flow," *Proceedings of the 16th International Federation of Automatic Control World Congress 2005 (IFAC 2005)*, Elsevier, New York, 2006.
[32] King, R., Becker, R., Garwon, M., and Henning, L., "Robust and Adaptive Closed-Loop Control of Separated Shear Flows," AIAA Paper 2004-2519, 2004.
[33] Annaswamy, A., Fleifil, M., Rumsey, J., Prasanth, R., Hathout, J., and Ghoniem, A., "Thermoacoustic Instability: Model-Based Optimal Control Design and Experimental Validation," *IEEE Transactions on Control Systems Technology*, Vol. 8, No. 6, 2000, pp. 905–918.
[34] Baumann, M., and Nitsche, W., "Investigation of Active Control of Tollmien-Schlichting Waves on a Wing," *Transitional Boundary Layers in Aeronautics*, Vol. 46, 1996, pp. 89–98.
[35] Henning, L., and King, R., "Drag Reduction by Closed-Loop Control of a Separated Flow over a Bluff Body with a Blunt Trailing Edge," *44th Institute of Electrical and Electronics Engineers (IEEE) Conference on Decision and Control and European Control Conference (ECC)*, IEEE, Piscataway, NJ, 2005.
[36] Cabell, R. H., Kegerisey, M. A., Coxz, D. E., and Gibbs, G. P., "Experimental Feedback Control of Flow Induced Cavity Tones," AIAA Paper 2002-2497, 2002.
[37] Rowley, C. W., and Williams, D. R., "Control of Forced and Self-Sustained Oscillations in the Flow Past a Cavity," AIAA Paper 2003-0008, 2003.
[38] Rapoport, D., Fono, I., Cohen, K., and Seifert, A., "Closed-Loop Vectoring Control of a Turbulent Jet Using Periodic Excitation," *Journal of Propulsion and Power*, Vol. 19, No. 4, 2003, pp. 646–654.
[39] Dovgal, A. V., Kozlov, V. V., and Michalke, A., "Contribution to the Instability of Laminar Separating Flows Along Axisymmetric Bodies. Part 2. Experiment and Comparison with Theory," *European Journal of Mechanics, B/Fluids*, Vol. 14, No. 3, 1995, pp. 351–365.
[40] Michalke, A., "Contribution to the Instability of Laminar Separating Flows Along Axisymmetric Bodies. Part 1. Theory," *European Journal of Mechanics, B/Fluids*, Vol. 14, No. 3, 1995, pp. 333–350.
[41] Helmholtz, H., *Ostwalds Klassiker der exakten Wissenschaften*, Chap. Über Diskontinuierliche Flüssigkeitsbewegungen, Harri Deutsch Verlag, Frankfurt, 1996.
[42] Huppertz, A., and Janke, G., "Some New Results on the Control of the Flow over a Backward-Facing Step," *Euromech Colloquium 361—Active Control of Turbulent Shear Flows*, Springer, Berlin, 1997.
[43] Chun, K. B., and Sung, H. J., "Visualization of a Locally-Forced Separated Flow over a Backward-Facing Step," *Experiments in Fluids*, Vol. 25, No. 2, 1998, pp. 133–142.
[44] Sigurdson, L. W., "The Structure and Control of a Turbulent Reattaching Flow," *Journal of Fluid Mechanics*, Vol. 298, 1995, pp. 139–165.
[45] Chun, S., Lee, I., and Sung, H. J., "Effect of Spanwise-Varying Local Forcing on Turbulent Separated Flow over a Backwardfacing Step," *Experiments in Fluids*, Vol. 26, No. 5, 1999, pp. 437–440.
[46] Fernholz, H. H., Janke, G., Schober, M., Wagner, P. M., and Warnack, D., "New Devolopments and Applications of Skin-Friction Measuring Techniques," *Measuring Science Technology*, Vol. 7, No. 10, 1996, pp. 1396–1409.
[47] Mabey, D. G., "Analysis and Correlation of Data on Pressure Fluctuations in Separated Flow," *Journal of Aircraft*, Vol. 9, No. 9, 1972, pp. 642–645.
[48] Kiya, M., and Sasaki, K., "Structure of a Turbulent Separation Bubble," *Journal of Fluid Mechanics*, Vol. 137, 1983, pp. 83–113.
[49] Cherry, N. J., Hillier, R., and Latour, M. E. M. P., "Unsteady Measurements in a Separated and Reattaching Flow," *Journal of Fluid Mechanics*, Vol. 144, 1984, pp. 13–46.
[50] Lee, I., and Sung, H. J., "Characteristics of Wall Pressure Fluctuations in Separated and Reattaching Flows over a Backward-Facing Step: Part 1. Time-Mean Statistics and Cross-Spectral Analysis," *Experiments in Fluids*, Vol. 30, No. 3, 2001, pp. 262–272.
[51] Hudy, L. M., Naguib, A. M., and Humphreys, W. M., "Wall-Pressure-Array Measurements Beneath a Separating/Reattaching Flow Region," *Physics of Fluids*, Vol. 15, No. 3, 2003, pp. 706–717.
[52] Becker, R., Garwon, M., and King, R., "Development of Model-Based Sensors and Their Use for Closed-Loop Control of Separated Shear Flows," *Proceedings of the European Control Conference (ECC) 2003*, ECC, Cambridge, U.K., 2003.
[53] Ljung, L., *System Identification—Theory for the User*, Prentice–Hall PTR, Upper Saddle River, NJ, 1999.
[54] Skogestad, S., and Postlethwaite, I., *Multivariable Feedback Control—Analysis and Design*, Wiley, Chichester, U.K., 1996.